ACQUIRED VITELLIFORM LESIONS

Correlation of Clinical Findings and Multiple Imaging Analyses

K. BAILEY FREUND, MD,*†‡ KETAN LAUD, MD,*†‡ LUIZ H. LIMA, MD,† RICHARD F. SPAIDE, MD,*† SANDRINE ZWEIFEL, MD,†§ LAWRENCE A. YANNUZZI, MD*†

Purpose: To correlate clinical observations with multimodal imaging analysis in acquired vitelliform lesions (AVLs) and to elucidate their nature, pathogenesis, and natural course.

Methods: Clinical examination, color fundus photography, fluorescein angiography, near-infrared reflectance, fundus autofluorescence, and spectral-domain optical coherence tomography (SD-OCT) data were retrospectively reviewed for a consecutive series of 90 eyes of 67 patients with an AVL secondary to a variety of diagnoses.

Results: In all 90 eyes with AVLs, SD-OCT helped localize the clinically apparent yellowish material to the subretinal space above the retinal pigment epithelial (RPE) band. Only 19 eyes (21.1%) had SD-OCT evidence of subretinal fluid. All eyes exhibited abnormal hyperautofluorescence corresponding to the material seen clinically. In 18 of 72 eyes (25.0%) imaged simultaneously with SD-OCT and near-infrared reflectance imaging, near-infrared hyperreflectivity corresponding to presumed collections of pigment-laden macrophages and RPE cells was observed. Resolution of some AVLs appeared to coincide with progressive thinning of the outer nuclear layer, indicating a gradual loss of photoreceptors. Visual acuity at baseline was best predicted by the subfoveal integrity of the external limiting membrane ($P = 0.001$) and the inner segment/outer segment junction ($P = 0.0002$) on SD-OCT. Fluorescein angiography revealed a pattern often mimicking poorly defined (Type 1) choroidal neovascularization.

Conclusion: Acquired vitelliform lesions occur in a variety of different clinical entities that share common features with multimodal imaging analyses. We propose that both dysfunctional RPE and loss of apposition between the photoreceptor tips and the RPE can interfere with the phagocytosis of shed outer segments. Both this material and pigment-laden macrophages and RPE cells appear to contribute to the yellowish appearance of AVLs. Ongoing photoreceptor loss may in some cases be associated with the spontaneous resolution of an AVL.

RETINA 31:13–25, 2011

Accumulations of yellowish and presumably subretinal material can occur in a variety of macular disorders. We refer to this finding generically as a vitelliform lesion (VL) to avoid confusion with the terms vitelliform macular dystrophy and vitelliform macular degeneration. Vitelliform lesions most commonly develop singly beneath the fovea but are occasionally multiple and can occur in other locations within the macular region. When detected in younger patients, VLs often occur in the setting of Best macular dystrophy (Best disease), an autosomal dominant disorder with variable penetrance and expressivity. Best disease has been associated with a mutation in bestrophin 1 (BEST1), a gene on 11q13 that codes for a transmembrane anion channel found on the basolateral plasma membrane of retinal pigment epithelial (RPE) cells.[1–3]

Multiple causative etiologies may produce an acquired vitelliform lesion (AVL), but only some

have known genetic associations. Inconsistent terminology prevails in the literature. The terms pattern dystrophy, adult-onset vitelliform macular detachment,[4] foveomacular vitelliform dystrophy—adult type,[5–7] pseudovitelliform macular degeneration,[8,9] and adult-onset foveomacular pigment epithelial dystrophy[10,11] are often used interchangeably in describing these eyes. Some specific genetic causes of AVLs have been identified, including mutations in either the Best 1 or the photoreceptor peripherin gene (*PRPH2/RDS*) on Chromosome 6 (6p21.1-cen).[12,13] When VLs present in adults without typical findings of age-related macular degeneration (AMD), the term ''pattern dystrophy'' is commonly used even in the absence of a known family history of AVLs or a proven mutation in one of the known associated genes. Other entities associated with AVLs include cuticular drusen, tractional maculopathies,[14] and AMD. The purpose of this investigation was to correlate clinical observations with multimodal imaging analysis in a large series of patients with AVLs due to multiple causes in order to elucidate the nature, pathogenesis, and natural course of this entity.

Methods

We analyzed clinical and imaging data from a consecutive series of 90 eyes of 67 patients with AVLs who came for a routine follow-up examination at the Vitreous-Retina-Macula Consultants of New York, a large group retinal practice based in New York City, NY, between January 2008 and October 2009. The Institutional Review Board of the Manhattan Eye, Ear, and Throat Hospital approved this retrospective review. Eyes were included if dilated funduscopic examination had detected the presence of an AVL in the macular region based on the following definition: presence of a well-circumscribed area of yellowish subretinal material detected in patients older than 40 years. Only eyes having previously undergone multimodal imaging analyses (high-resolution digital color fundus photographs, fundus autofluorescence [FAF], fluorescein angiography [FA], and spectral-domain optical coherence tomography [SD-OCT]) were included. Patients with a known family history of Best macular dystrophy were excluded. The presence of cuticular drusen was based on FA demonstrating the typical ''stars in the sky'' or ''milky way'' pattern of multiple small hyperfluorescent spots and multiple small hypoautofluorescent spots on FAF imaging. Nonneovascular AMD was defined by the presence of drusen with or without retinal pigment epithelial detachment (PED) (drusenoid or serous), geographic atrophy, and pigment hyperplasia. No eyes with

evidence of choroidal neovascularization (CNV) at baseline, based on clinical examination, FA, and SD-OCT, were included in this series.

High-resolution digital color fundus photographs and FA were obtained with the Topcon TRC-50XF fundus camera (Topcon Medical Systems; Paramus, NJ). The greatest linear dimension (GLD) of the AVLs was measured using the caliper function with the confocal scanning laser ophthalmoscope (Heidelberg Retina Angiograph, HRA2; Heidelberg Engineering, Heidelberg, Germany). Fundus autofluorescence images were obtained using either the confocal scanning laser ophthalmoscope (Heidelberg Retina Angiograph, HRA2; Heidelberg Engineering) with an excitatory light of 488 nm and emitted light above 500 nm detected using a barrier filter or the Topcon autofluorescence filters (excitation filter centered at 560 nm [bandwidth, 535–585 nm] and a barrier filter centered at 655 nm [bandwidth, 615–715 nm]) with the Topcon TRC-50XF fundus camera (Topcon Medical Systems). Near-infrared reflectance (nIR) images were obtained with the confocal scanning laser ophthalmoscope (Heidelberg Retina Angiograph, HRA2; Heidelberg Engineering) using a light stimulus of 815 nm. Spectral-domain optical coherence tomographic examinations were performed using either the 3D-OCT 1000 (Topcon, Tokyo, Japan) or the Spectralis HRA + OCT (Heidelberg Engineering), which has integrated eye tracking, allowing for live averaging of confocal scanning laser ophthalmoscope images (nIR and FAF) and optical coherence tomographic B-scans. The SD-OCT scans were positioned within the macular area and were topographically correlated with the color fundus photographic, nIR, FA, and FAF images. For each scan, qualitative data including shape, size, and reflectivity of the abnormal material, its location about the RPE and retinal layers, and the reflectivity and appearance of the RPE were recorded. In a subset of 72 eyes of 50 patients, quantitative measurements of several anatomical features were recorded using the calipers provided in the review software of the Spectralis HRA + OCT. For the remaining 18 eyes of 17 patients imaged with only the 3D-OCT 1000, the individual B-scan resolution was judged to be inadequate for these measurements. Height of the AVLs was measured from the apical surface to the RPE to the external limiting membrane (ELM) or (when the ELM was absent) the posterior border of the outer nuclear layer (ONL). Caliper measurements were recorded for ONL thickness at the fovea. Presence or absence of a discernable ELM and inner segment/outer segment (IS/OS) junction at the foveal center were recorded for each eye.

The individual effects of GLD of the AVLs, ONL thickness at the fovea, and AVL height on visual acuity were analyzed using linear regression. Visual acuities were converted to logarithm of the minimum angle of resolution units before any calculations. The associations of ELM and IS/OS with visual acuity were evaluated through analysis of variance models. The correlation between ELM status and IS/OS junction status was analyzed using the chi-square test. A P value of <0.05 was considered statistically significant.

Results

We evaluated 90 eyes of 67 patients who met the inclusion criteria and had previous multimodal imaging analyses over a follow-up ranging from 2 months to 24 months. There were 38 female and 29 male subjects ranging in age from 45 years to 93 years (mean age: 72 years) at the time the AVL was first imaged with multimodal analyses. All the patients were white. In all eyes, the AVLs occurred in the central macula and involved the foveola. Forty eyes (44.4%) of 28 patients (mean age: 73 years) had an AVL without any other clinically apparent funduscopic abnormalities (less than Age-Related Eye Disease Study Category 2).[15] Twenty eyes (22.2%) of 14 patients (mean age: 74 years) had an AVL in association with cuticular drusen. Nineteen eyes (21.1%) of 16 patients (mean age: 79 years) had an AVL in association with nonneovascular AMD (Age-Related Eye Disease Study Category 2 or greater) (Figure 1). Three eyes (3.3%) of 2 patients (mean age: 85 years) had subretinal drusenoid deposits (reticular pseudodrusen)[16] based on clinical examination, FAF, and SD-OCT findings (Figure 1). Three eyes (3.3%) of 2 patients (mean age: 61 years) had an AVL associated with pseudoxanthoma elasticum (PXE) and angioid streaks (Figure 1). Three eyes (3.3%) of 3 patients (mean age: 75 years) had an AVL in association with vitreomacular traction (Figure 1). Two eyes (2.2%) of 2 patients (mean age: 55 years) had an AVL associated with central serous chorioretinopathy (CSC) (Figure 1).

In 7 eyes (7.7%) of 7 patients, the AVL was detected overlying a retinal PED, 3 of which were serous and 4 of which were drusenoid. Of the seven patients with a PED, four had nonneovascular AMD, one had cuticular drusen, and two had no other funduscopic abnormalities.

Best-corrected visual acuity at the time the AVL was first imaged with multimodal imaging ranged widely from 20/20 to 3/400 (median acuity: 20/50). Forty-four eyes (48.8%) had visual acuity of 20/40 or better. Forty-two eyes (46.6%) had visual acuities of 20/50 to 20/150, and 4 eyes (4.4%) were legally blind (20/200 or worse). The most common visual complaints noted were slowly progressive decline in visual acuity, metamorphopsia, decreased reading vision, mild photophobia, and central or paracentral visual field defects. Thirty-seven eyes (41.1%) of 26 patients had ≥6 months (range: 6–22 months; mean: 11 months) of follow-up. In these eyes, mean visual acuity at the time of AVL diagnosis was 20/59 (median: 20/40) and at the most recent examination was 20/68 (median: 20/40). Ten eyes (11.1%) had visual acuity improvement over the follow-up period.

Forty-one patients (45.5%) were taking nutritional supplements, 6 patients (6.6%) had received previous treatment with topical dorzolamide 2%, 13 patients (14.4%) had received ≥1 intravitreal anti–vascular endothelial growth factor injections of either ranibizumab (0.5 mg/0.05 mL) or bevacizumab (1.25 mg/0.05 mL). In all patients treated with intravitreal anti–vascular endothelial growth factor therapy, treatment was discontinued after a mean of 4 injections because of a lack of perceived benefit in anatomical outcome or visual acuity.[17]

In all 90 eyes with AVLs, SD-OCT localized the clinically apparent yellowish lesion to hyperreflective material in the subretinal space above the RPE band (Figures 2 and 3). In the cohort of 72 eyes imaged with the Spectralis HRA + OCT, the subretinal material was bounded anteriorly by the photoreceptor IS/OS junction in 47 eyes (65.3%), and in 25 eyes (34.7%) with more chronic lesions, a defined IS/OS junction at the foveal center could not be identified above the vitelliform material on SD-OCT. In these eyes, the hyperreflective vitelliform material was bounded anteriorly by the ELM. At the last follow-up visit, in 14 eyes (19.4%), the ELM was absent at the foveal center. The vitelliform material in these eyes was bounded anteriorly by the ONL.

In the 72 eyes imaged with the Spectralis HRA + OCT, the GLD of the AVLs ranged from 192 μm to 3,839 μm (mean: 975 μm) at baseline, decreasing to a mean of 747 μm at the last follow-up. Visual acuity was inversely correlated with the baseline GLD at both the baseline ($P = 0.02$) and the last follow-up visits ($P = 0.0007$). The baseline height (distance from the apical border of the RPE to the ELM or, when absent, the posterior border of the ONL) of the AVLs ranged from 39 μm to 628 μm (mean: 185 μm) at baseline, decreasing to a mean of 152 μm at the last follow-up. Visual acuity was inversely correlated with the baseline AVL height at both the baseline ($P = 0.02$) and the last follow-up visits ($P = 0.002$). Thickness of the ONL at the foveal center ranged from 0 μm to 175 μm (mean: 78.8 μm) at baseline. In 37 eyes having ≥6 months (mean: 11 months) of follow-up scanning on the Spectralis HRA + OCT, there was a gradual
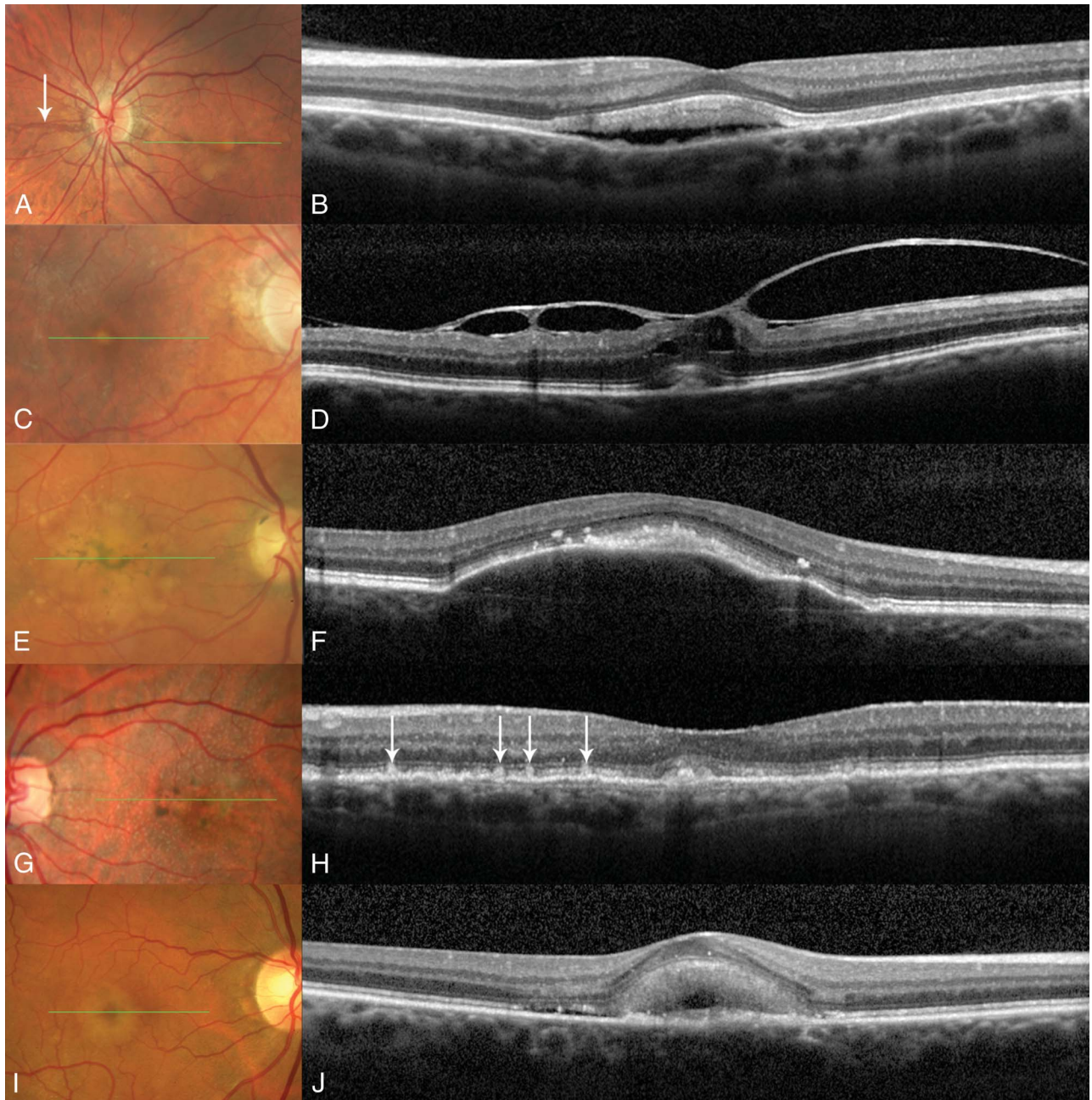
Fig. 1. Varied presentations of AVLs. **A.** Color photograph showing an AVL in the left eye of a patient with PXE and angioid streaks (arrow). **B.** Corresponding SD-OCT B-scan through the AVL in the eye shown in (**A**) (green line). There is SRF and hyperreflective material in the subretinal space adherent to a diffusely thickened IS/OS junction. Focal thickenings or bumps are noted above the RPE band. The ONL and ELM are preserved in this eye with 20/20 visual acuity. **C.** Color photograph showing a small AVL and an epiretinal membrane in an eye with vitreomacular traction. **D.** Corresponding SD-OCT B-scan through the AVL shown in (**C**) (green line). There is tractional elevation of the fovea with cystic changes of the inner retina. There is hyperreflective material in the subretinal space and a focal thickening or bump involving the RPE band. **E.** Color photograph showing an AVL with RPE hyperplasia overlying a retinal PED in the right eye of a patient with nonneovascular AMD. There are multiple drusen surrounding the PED. **F.** Corresponding SD-OCT B-scan through the AVL (green line in **E**) showing hyperreflective material in the subretinal space overlying a serous retinal PED. There are focal thickening or bumps involving the RPE band and two small hyperreflective foci present in the ONL. **G.** Color photograph showing an AVL in an eye with subretinal drusenoid deposits (reticular pseudodrusen). **H.** Corresponding SD-OCT B-scan through the AVL shown in (**G**) (green line). There is a small AVL beneath the fovea and several subretinal drusenoid deposits (arrows). **I.** Color photograph showing an AVL in an eye with CSC. **J.** Corresponding SD-OCT B-scan through the AVL shown in (**I**) (green line). There is an AVL beneath the fovea, a small amount of SRF at the temporal edge of the AVL, and a thick choroid.

Fig. 2. Multimodal imaging in a large AVL. **A.** Fundus autofluorescence image of a large AVL (same eye as Figure 5I) with a GLD of 1,652 μm showing a well-circumscribed area of hyperautofluorescence corresponding to the clinically visible yellowish material in an eye with an AVL but no other funduscopic abnormalities. **B.** Near-infrared reflectance image showing hyperreflectivity within the AVL corresponding to focal thickenings and bumps involving the RPE band on the corresponding SD-OCT (**E**). The circular area of hyperreflectivity centrally is an artifact (arrow). **C.** Corresponding recirculation-phase fluorescein angiogram showing blocked fluorescence inferiorly by material within the subretinal space. **D.** Corresponding recirculation-phase FA showing diffuse staining of the AVL. The angiographic pattern resembles that of occult (Type 1) CNV. **E.** Corresponding SD-OCT B-scan through the AVL (green line in **B**) showing hyperreflective material in the subretinal space, focal thickening or bumps involving the RPE band, partial disruption of the IS/OS junction, preservation of the ELM, and thinning of the ONL. **F.** Corresponding schematic drawing showing shed photoreceptor outer segments and clumps of pigment-laden RPE cells and macrophages in the subretinal space. There is thinning of ONL with relative preservation of the photoreceptor outer segments.
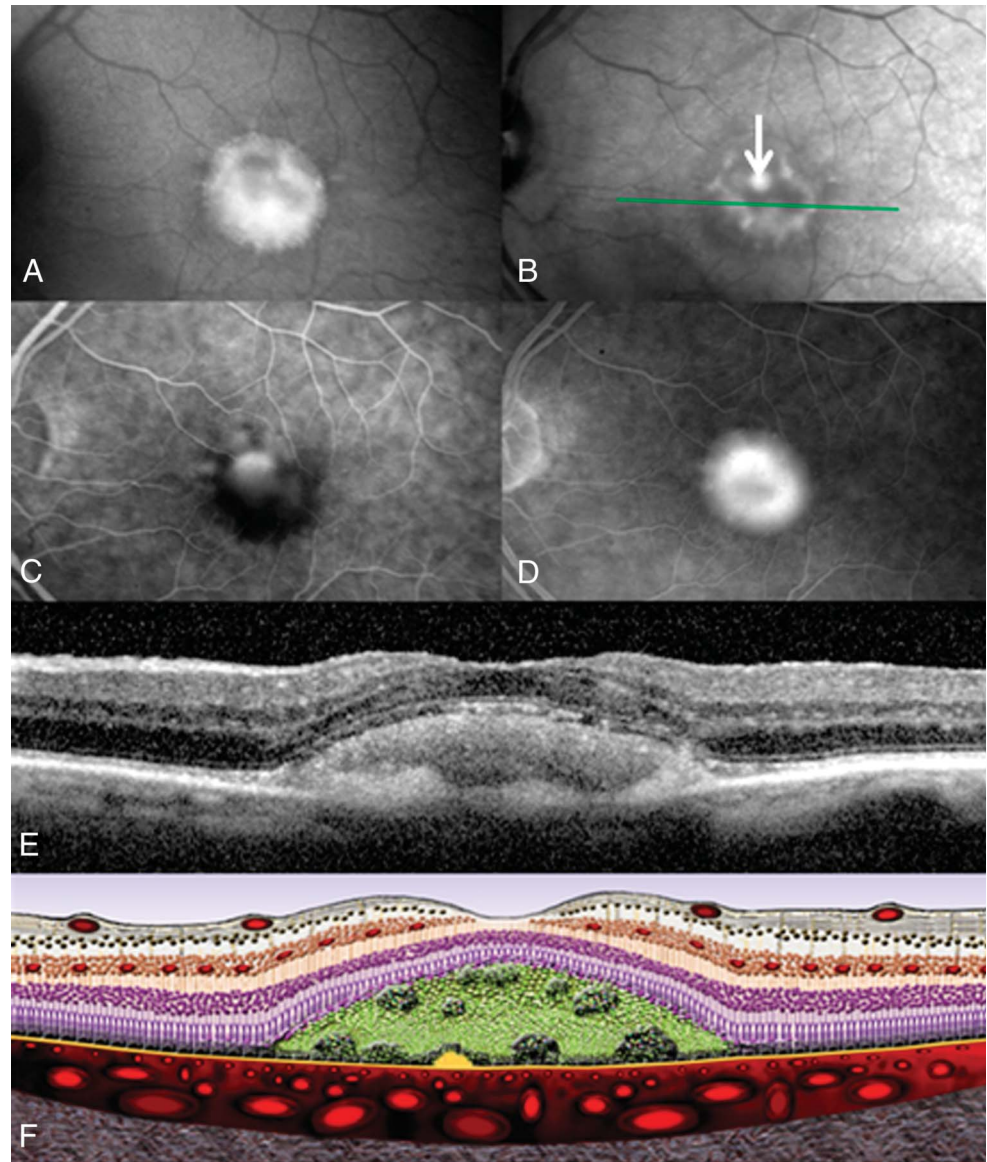
decline in ONL thickness. Mean ONL thickness at the foveal center decreased to a mean of 66.8 μm at the last follow-up examination. The mean decrease in ONL thickness over the follow-up period was 9.67 μm. The ONL thickness at baseline and at the last follow-up had no significant effect on either baseline ($P = 0.25$) or last follow-up ($P = 0.15$) visual acuity. There was a highly significant inverse correlation between visual acuity and absence of a discernible IS/OS junction beneath the foveola both at the baseline ($P = 0.0002$) and at the last follow-up ($P = 0.0001$). There was also a highly significant inverse correlation between visual acuity and absence of a discernable ELM beneath the foveola both at the baseline ($P = 0.001$) and at the last follow-up ($P = 0.0001$). The

correlation between ELM status and IS/OS junction status was highly significant ($P = 0.0001$).

In 71 eyes (78.8%), SD-OCT did not detect evidence of subretinal fluid (SRF), while in 19 eyes (21.2%), SD-OCT detected a hyporeflective space consistent with SRF (Figures 1 and 4). Of the 19 eyes with SRF, 8 eyes (42.1%) had no other fundus abnormalities, 5 eyes (26.3%) had cuticular drusen, 3 eyes (15.8%) had nonneovascular AMD, 2 eyes (10.5%) had PXE, and 1 eye (5.3%) had CSC. When present, SRF occurred between the "vitelliform material" accretion, which appeared to adhere to the underside of the retina, and the RPE. Only a single eye of 1 patient with PXE developed a meniscus of material similar to the pseudohypopyon seen in Best macular dystrophy (Figure 1).
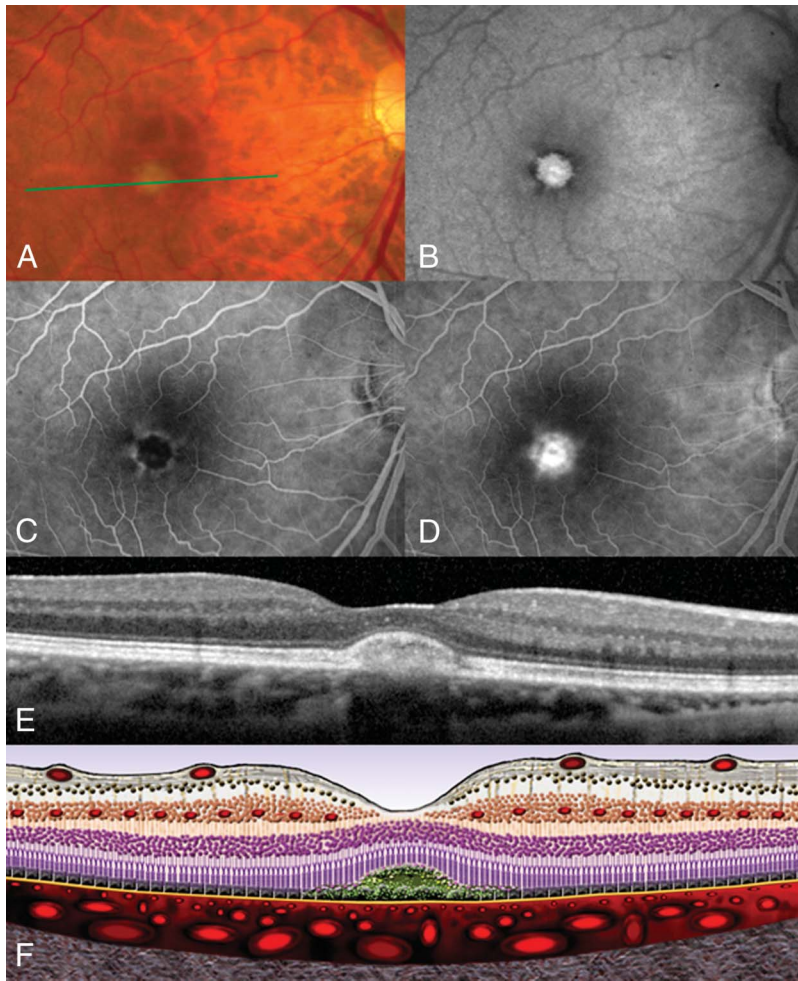
Fig. 3. Multimodal imaging in a small AVL. **A.** Color photograph showing a small AVL (GLD = 505 μm) in an eye with no other fundus abnormalities. **B.** Fundus autofluorescence image showing hyperautofluorescence, which corresponds to the yellowish material in the color photograph (**A**) and the material in the subretinal space (**E**). **C.** Corresponding transit-phase fluorescein angiogram showing blocked fluorescence by material with the subretinal space. **D.** Corresponding recirculation-phase FA showing diffuse staining of the AVL. The angiographic pattern resembles that of occult (Type 1) CNV. **E.** Spectral-domain optical coherence tomography shows hyperreflective material within the subretinal space. There is thickening of an intact IS/OS junction, preservation of the ELM, and mild thinning of the ONL. There is no evidence of SRF. **F.** Corresponding schematic drawing showing shed photoreceptor outer segments and clumps of pigment-laden RPE cells and macrophages in the subretinal space. There is mild thinning of ONL with relative preservation of the photoreceptor outer segments.

We did not identify any early lesions with SRF or any unilateral AVLs in which the fellow eye had SRF in the absence of an AVL. Intraretinal fluid or cystic intraretinal spaces were identified in a single eye with vitreomacular traction (Figure 1).

Of 90 eyes, from the entire 67 patient cohort, with a follow-up of >6 months, 12 eyes (13.3%) developed spontaneous regression of the AVLs. In these 12 eyes experiencing a spontaneous regression of the AVL, mean visual acuity at baseline was 20/60 and decreased to 20/80 at the last follow-up after resolution of the AVL. Three eyes experienced visual improvement after the spontaneous regression of the AVL. After resolution of the AVL, all eyes manifested varying degrees of atrophic changes on SD-OCT, including thinning and focal loss of the ONL, disruptions in IS/OS junction and ELM, and thinning or focal loss of the RPE band, which correlated with hypoautofluorescence on FAF (Figure 5).

Focal thickening or bumps above the RPE band on SD-OCT occurred in 18 eyes (20.0%) of the patient cohort imaged with the Spectralis HRA + OCT (Figures 2 and 4). Focal thickening of the RPE band was seen in nine eyes having AVLs without other funduscopic abnormalities, five eyes with cuticular drusen, two eyes with nonneovascular AMD, one eye with CSC, and one eye with PXE. These areas of focal RPE thickening correlated with pigment hyperplasia present on color fundus photographs and appeared to be located beneath the yellowish subretinal material. Unlike the yellowish material, the pigment hyperplasia was intensely hyperreflective with nIR reflectance imaging on the scanning laser ophthalmoscope, consistent with a high concentration of melanin (Figure 2). In 2 eyes with nonneovascular AMD and 2 eyes with AVL without other funduscopic abnormalities, the hyperreflective material appeared to have migrated into the overlying neurosensory retina (Figures 6 and 7).

All the AVLs exhibited hyperautofluorescence that correlated with the material in the subretinal space on SD-OCT (Figures 2 and 3). In the 12 eyes with

Fig. 4. Multimodal imaging in cuticular drusen associated with an AVL. **A.** Color photograph showing an AVL (GLD = 839 μm) in an eye with cuticular drusen. **B.** Fundus autofluorescence image showing multiple small hypoautofluorescence dots that correspond to the cuticular drusen. There is weak hyperautofluorescence corresponding to the yellowish material in the color photograph (**A**). **C** and **D.** Corresponding transit-phase (**C**) and recirculation-phase (**D**) fluorescein angiogram showing the characteristic "stars in the sky" pattern of cuticular drusen. The angiographic pattern of the AVL resembles that of occult (Type 1) CNV. **E.** Spectral-domain optical coherence tomography shows hyper-reflective material beneath the IS/OS junction, subretinal fluid, and multiple thickenings or bumps of the RPE band. **F.** Corresponding schematic drawing showing shed photoreceptor outer segments and clumps of pigment-laden RPE cells and macrophages in the subretinal space. Some of these cells have migrated to the overlying neurosensory retina. There is thinning of the ONL with relative preservation of the photoreceptor outer segments.
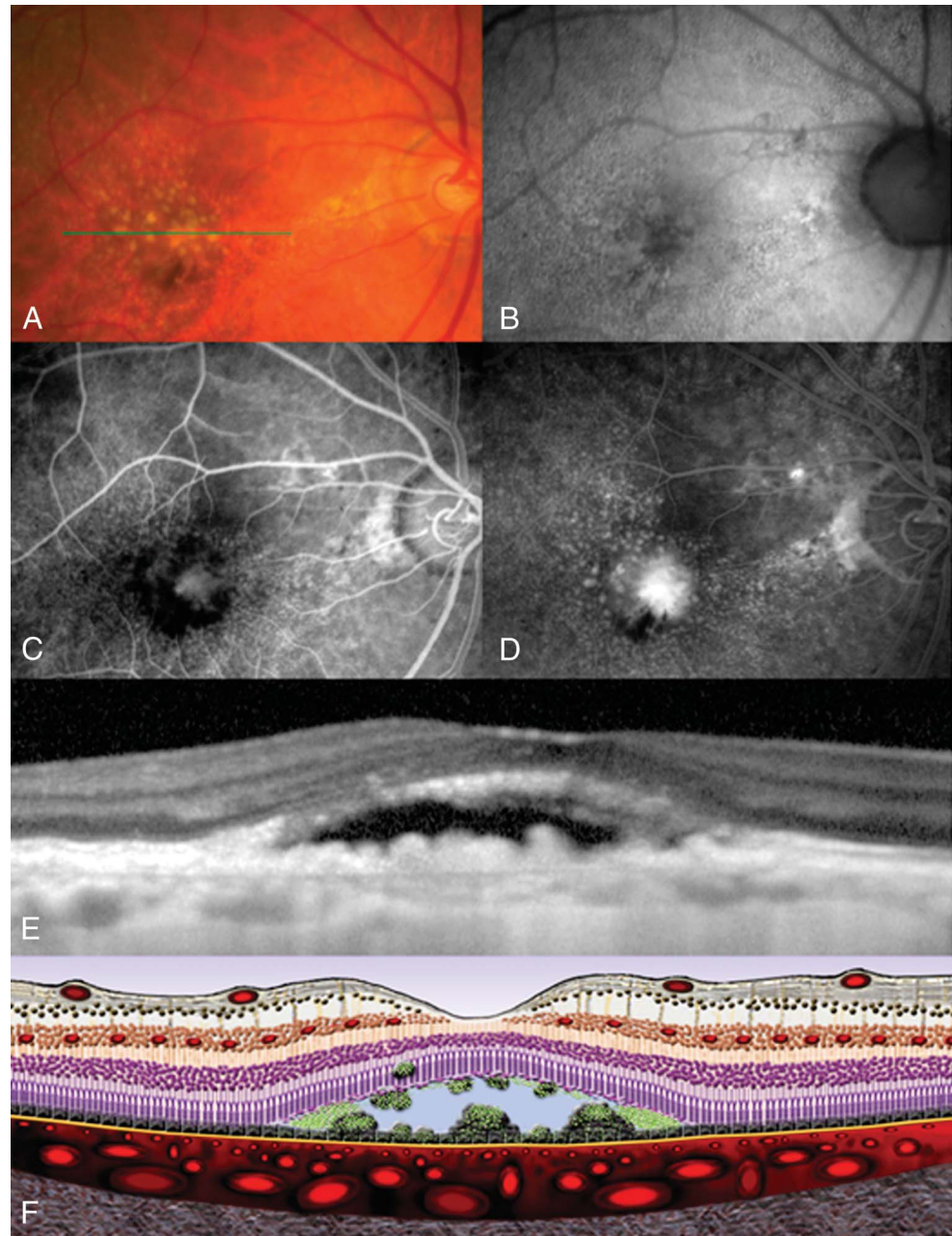
spontaneous regression of the AVL, FAF showed hypoautofluorescence centrally, indicative of RPE loss with a hyperautofluorescent border. The very small hypoautofluorescent lesions of cuticular drusen seen on FAF corresponded to the hyperfluorescent spots ("stars in the sky") on FA (Figure 4).

Fluorescein angiography of the AVLs revealed hypofluorescence (blocked fluorescence) because of the subretinal material during the dye transit. Late hyperfluorescence (staining) of the subretinal material was present in the recirculation phase of the FA (Figures 2 and 3). In many eyes, these angiographic findings mimicked the pattern seen in AMD eyes harboring Type 1 (occult, poorly defined) neovascularization. No study eyes developed FA, clinical, fundus photographic, or SD-OCT evidence of CNV during the follow-up period.

Discussion

Adult VLs may occur in a variety of different entities that share common imaging features regardless of the underlying clinical diagnosis. A review of the multimodal imaging analyses of AVLs helps in the
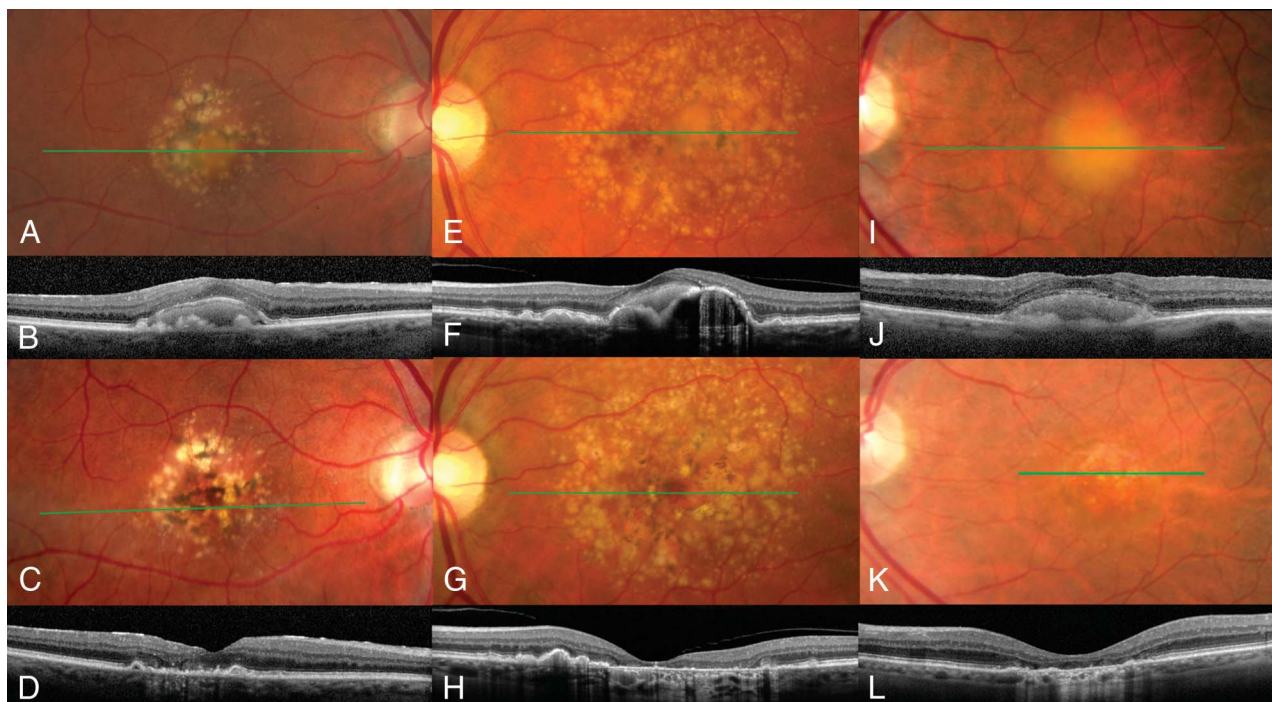
Fig. 5. Natural course of AVLs. **A.** Color photograph showing an AVL in association with multiple drusen and RPE hyperplasia. **B.** Corresponding SD-OCT showing thinning of the ONL overlying an accumulation of hyperreflective material in the subretinal space. There are focal thickenings or bumps of the RPE band. **C.** Color photograph of the same eye 27 months later shows resolution of the vitelliform material exposing areas of RPE atrophy and persistent RPE hyperplasia. **D.** Corresponding SD-OCT shows resolution of the subretinal material, atrophy of the RPE, and discontinuity of the overlying IS/OS junction and ELM temporal to the foveal depression. **E.** Color photograph of the left eye of a second patient with an AVL associated with cuticular drusen, large drusen, and RPE hyperplasia. **F.** Corresponding SD-OCT showing a PED with hyperreflective material in the subretinal space. There is marked thinning of the ONL. **G.** Color photograph of the same eye 15 months later shows resolution of the vitelliform material exposing RPE atrophy. **H.** Corresponding SD-OCT shows resolution of the subretinal material with loss of the photoreceptors overlying RPE atrophy. **I.** Color photograph of the left eye of a third patient showing an AVL with minimal additional age-related findings. **J.** Corresponding SD-OCT shows hyperreflective material in the subretinal space anterior to focal thickenings or bumps of the RPE band. **K.** Color photograph of the same eye 10 months later shows resolution of the vitelliform material beneath the fovea exposing RPE atrophy. **L.** Corresponding SD-OCT reveals loss of the IS/OS junction with underlying RPE atrophy, absence of the ELM, and marked thinning of the ONL.

understanding of the mechanisms involved in the formation of these lesions and in recognizing the pertinent features associated with visual function and long-term prognosis. Distinguishing AVLs from CNV can avert unnecessary interventions and the risks associated with such treatments.

In our cohort of 90 eyes of 67 patients, AVLs in the absence of other funduscopic abnormalities were the most frequent (44.4% of eyes) presentation. The mean age at baseline of these cases was 73 years. The AVLs were present bilaterally in 43% of these patients who were typically given the clinical diagnosis of a pattern dystrophy or adult-onset foveomacular dystrophy. Cuticular drusen was the second most frequent association (22.2% of eyes). These eyes often manifested additional findings of AMD, including large drusen and pigment hyperplasia. The AVLs occurred bilaterally in 43% of these patients. Non-neovascular AMD without cuticular drusen was the third most frequent association (21.1% of eyes) occurring bilaterally in only 19% of these patients.

The mean age at baseline for these cases was 79 years. Acquired vitelliform lesions were identified in 3 eyes (3.3%) of 2 patients with PXE and angioid streaks, 3 eyes (3.3%) of 3 patients with vitreomacular traction, 2 eyes (2.2%) of 2 patients with subretinal drusenoid deposits (reticular pseudodrusen), and 2 eyes (2.2%) of 2 patients with CSC.

Adult VLs were typically round yellowish lesions with a GLD ranging from 192 μm to 3,939 μm (mean: 975 μm) and height ranging from 57 μm to 628 μm (mean: 185 μm). Visual acuity at both the baseline and the last follow-up visits was inversely correlated with the baseline GLD and height of the AVLs. In eyes with >6 months of follow-up, we observed a progressive thinning of the ONL, although the correlation of ONL thickness with visual acuity did not achieve statistical significance. This finding suggests that eyes with AVLs can maintain fairly good visual acuity despite considerable photoreceptor loss. A highly significant inverse correlation between visual acuity and loss of a discernable IS/OS junction and/or ELM band on
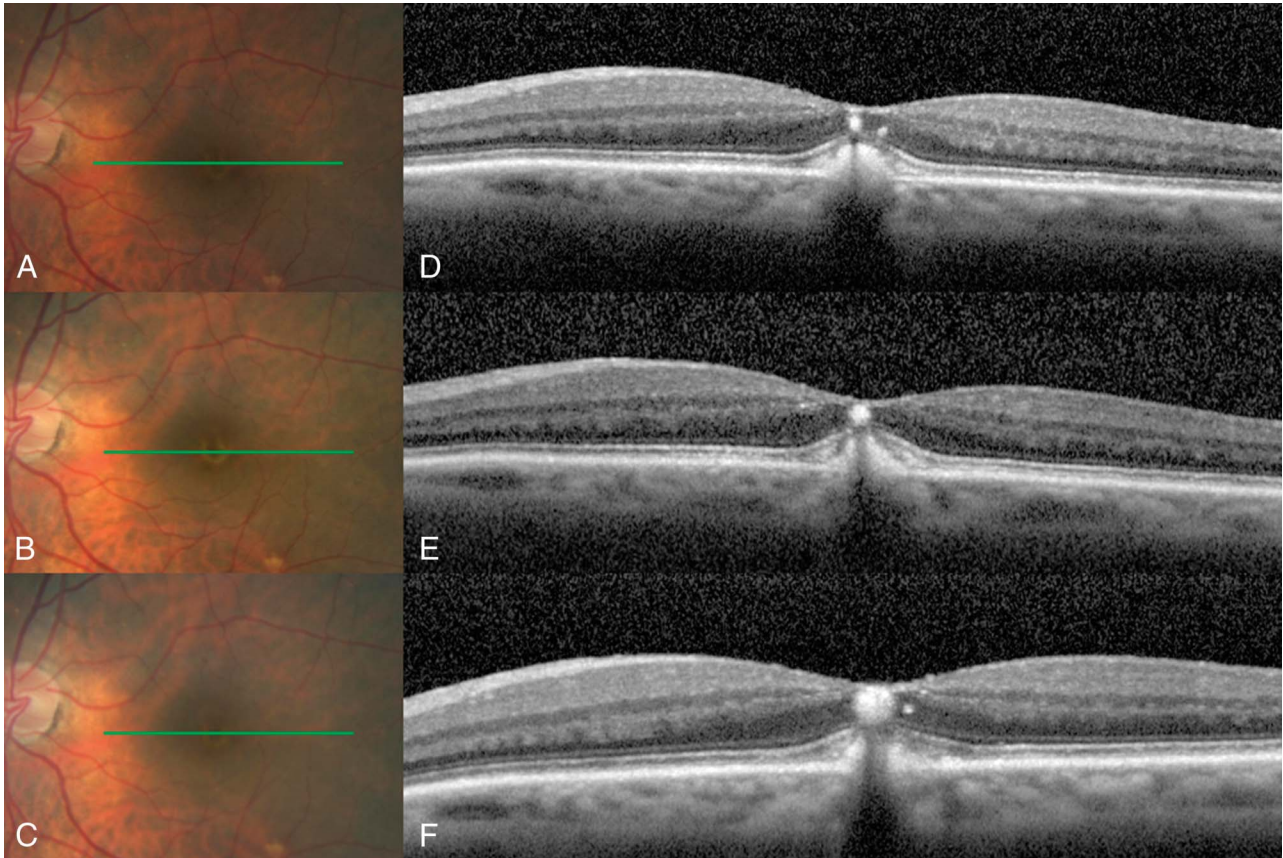
Fig. 6. Intraretinal migration of presumed pigment-laden cells in an AVL. **A–C.** Color photographs at baseline (**A**), 4 months (**B**), and 11 months (**C**) show a small AVL with associated RPE hyperplasia. **D–F.** Corresponding eye-tracked SD-OCT scans show a gradual increase in hyperreflective intraretinal material overlying the AVL. The intraretinal material is believed to represent pigment-laden RPE cells or macrophages.

SD-OCT suggests that the disruption of the photoreceptor outer segments is what accounts for much of the vision loss occurring in eyes with AVLs.

The multimodal imaging findings in our study helped clarify that the location of the clinically and photographically apparent subretinal yellowish material is in the subretinal space. Early reports correlating optical coherence tomography and other multimodal imaging findings in AVLs with the published histopathologic correlations were somewhat controversial.[18] Pierro et al[19] used early-generation time-domain optical coherence tomography (TD-OCT) to study 72 eyes of 43 patients with AVLs. They observed ''well-defined central subretinal thickening'' in all eyes with AVLs but recognized that the resolution of the older optical coherence tomography technology used did not allow for further characterization of this material.[19] Benhamou et al also used early-generation TD-OCT to study 21 eyes of 14 patients with AVLs. They concluded that in 16 eyes exhibiting late staining of the lesions on FA, the TD-OCT demonstrated that the vitelliform material was in the subretinal space bounded by the photoreceptor and RPE layers.[20] In the

remaining five eyes, they believed the vitelliform material was a focal thickening of the RPE layer that did not stain on FA. In a subsequent case report using third-generation TD-OCT (OCT3; Carl Zeiss Meditec, Inc., Dublin, CA), Benhamou et al localized the vitelliform material to the subretinal space in a single eye with an AVL.[21]

With the enhanced resolution of SD-OCT, the subretinal location of the abnormal material in VLs is more clearly demonstrated.[22,23] In our series, using exclusively SD-OCT, we localized the clinically apparent yellowish material to a distinct layer of hyperreflective material above the RPE band elevating the overlying neurosensory retina in all 90 eyes in the series.

The precise nature of the yellowish material in AVLs has also been a matter of some controversy and may vary depending on the underlying clinical setting. While there have been several published clinicopathologic correlations in eyes with various presentations of AVLs, a common finding in these reports has been varying amounts of lipofuscin and melanolipofuscin granules in the RPE and in macrophages detected in
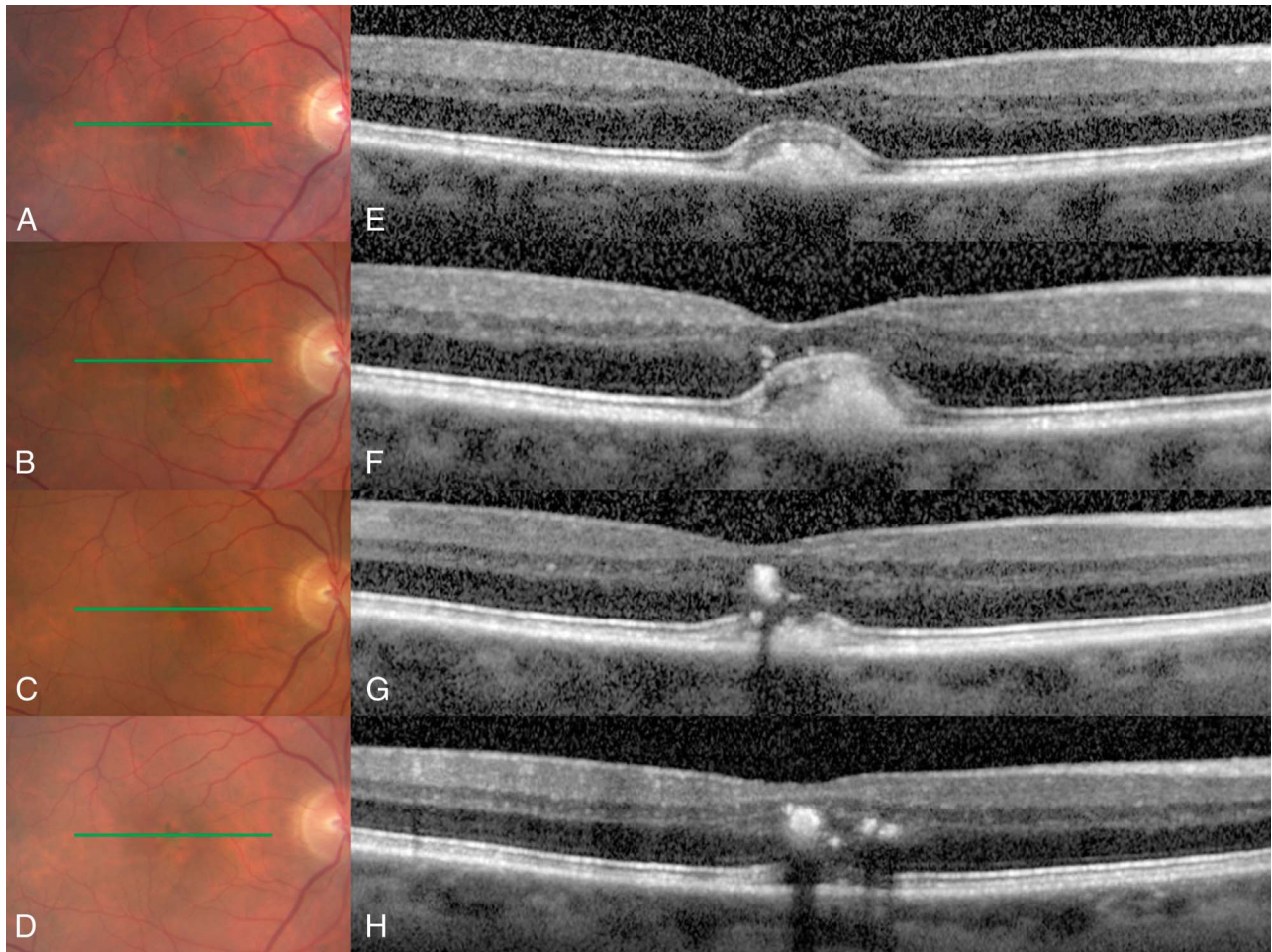
Fig. 7. Intraretinal migration of presumed pigment-laden cells in AVLs. **A–D.** Color photographs at baseline (**A**), 7 months (**B**), 9 months (**C**), and 15 months (**D**) show a small AVL with RPE hyperplasia. **E–H.** Corresponding eye-tracked SD-OCT scans show a gradual increase in intraretinal hyperreflective material overlying the AVL. There is a corresponding decrease in subretinal material.

the subretinal space. Dubovy et al[24] concluded that these pigmented cells had accounted for the yellowish vitelliform appearance in the eyes they studied postmortem; however, these eyes had relatively small accumulations of clinically apparent yellowish material. More recently, Arnold et al[25] reported a clinicopathologic analysis of 14 eyes with AVLs, concluding that extracellular material derived from the photoreceptor outer segment disks accounted for the majority of the subretinal material in these eyes. They hypothesized that defective phagocytosis of the photoreceptor tips by the RPE may lead to the accumulation of this material.

Additional histopathologic findings in eyes with AVLs have included varying degrees of central RPE attenuation and loss, loose pigment granules, loss of the RPE apical villi, intraretinal migration of pigment-laden cells, thinning of the ONL with varying degrees of outer segment thinning and loss, basal laminar and basal linear deposits, clumps of pigmented cells above

the RPE, and relative preservation of Bruch membrane and the choriocapillaris.[5,7,24,26,27] While many of these histopathologic findings are similar to those seen postmortem in younger patients with VLs due to Best macular dystrophy, basal laminar and basal linear deposits are less likely to be seen in younger patients.

While SD-OCT helps clarify the location of the yellowish material in AVL, other imaging modalities including FAF and nIR reflectance are useful here (as in various other disorders) for looking at the composition and suggesting the underlying pathophysiology.[28–31] The finding of abnormal FAF hyperautofluorescence in all eyes, which corresponded to the yellowish material seen clinically and with the material in the subretinal space on SD-OCT, suggests that this material originates at least in part from the photoreceptor outer segments. Although Parodi et al[32] performed a comparative analysis of FAF patterns and functional response using microperimetry in eyes with AVLs, this study did not incorporate optical coherence

tomography. Consequently, all hyperautofluorescent abnormalities in FAF were assumed to originate from lipofuscin granules within RPE cells. Three distinct autofluorescence patterns (normal, focal, and patchy) were observed with subjects manifesting the patchy autofluorescence pattern having the worst functional outcomes.[32] Furino et al[33] correlated FAF with TD-OCT (OCT3) findings in eyes with AVLs. They noted that the vitelliform material localized to the subretinal space and described several different patterns of abnormal FAF (patchy, ring-like, focal, and linear). They did not find a correlation between visual acuity and these FAF patterns.[33] In our study, multimodal imaging demonstrated that abnormal hyperautofluorescence in eyes with AVLs localizes not only to the RPE but also to the material in the subretinal space.

Autofluorescent precursors of lipofuscin including A2E and its primary precursors A2PE-H2, A2PE, and A2-rhodopsin can be found in the outer segments before phagocytosis by the RPE.[34,35] We believe our findings support the hypothesis that RPE dysfunction occurring in a variety of different macular disorders results in impaired turnover of the shed photoreceptor outer segments leading to an accumulation of this material in the subretinal space, most commonly extracellularly.[25] The accumulation of this vitelliform material, and in some cases SRF, would further impair turnover of the photoreceptor outer segments because of a loss of apposition between the photoreceptor tips and the apical surface of the RPE. Loss of apposition between the photoreceptors and the RPE has previously been implicated in accumulation of degenerating hyperautofluorescence material of photoreceptor origin in Best macular dystrophy, CSC, and optic pit maculopathy.[36,37] Presumably, this mechanism contributed to the formation of AVLs in our 2 eyes with vitreomacular traction and may help explain the common clinical finding of the yellow foveal appearance in eyes with Stage I macular holes (Figure 1).

Multimodal imaging in eyes with AVLs identified a second distinct type of material within the subretinal space believed to represent clusters of pigment-laden RPE cells and macrophages. Areas of presumed pigment hyperplasia noted on clinical examination, color fundus photographs, and FAF correlated with hyperreflective focal thickenings or bumps of the RPE band on SD-OCT in 18 eyes (20.0%) (Figures 2 and 4). These bumps were intensely reflective on nIR reflectance, suggesting a high content of melanin supporting a possible origin from the RPE monolayer in the form of RPE hyperplasia or macrophages containing large amounts of melanolipofuscin granules.[25,38] It appeared that this pigmented material may, in some eyes, migrate into the overlying neurosensory

retina where it can be detected on SD-OCT as hyperreflective bodies in several different retinal layers exhibiting nIR hyperreflectivity (Figures 6 and 7).

An additional multimodal imaging finding was the presence of a PED in 7 (7.7%) of the study eyes (Figures 1 and 5), most commonly with nonneovascular AMD. This finding further supports the subretinal location of the material in AVLs because the hyperreflective material corresponding to the yellowish hyperautofluorescent material was found above the elevated RPE band on SD-OCT.

Unlike some other entities associated with VLs, such as Best macular dystrophy and acute exudative polymorphous vitelliform maculopathy, SD-OCT evidence of SRF appeared to be a relatively infrequent finding in the AVLs of our series.[19,28,31] Subretinal fluid was detected with SD-OCT in only 21.1% of eyes, most of which had fairly chronic lesions with a mean ONL thickness of 67.3 μm. In eyes with SRF, there was typically hyperreflective material adherent to the underside of the retina, suggesting its origin from the photoreceptors as degenerating shed outer segments possibly as both extracellular and intracellular accretions (Figures 1 and 4). Only one eye, in a patient with PXE, had a meniscus of yellow material similar in appearance to the pseudohypopion stage of Best macular dystrophy, suggesting that this particular presentation is a rare occurrence in AVL. The absence of SRF in all the fellow eyes of these patients suggested that the accumulation of hyperreflective material in the subretinal space precedes that of SRF in many eyes with AVL. We believe that RPE dysfunction impairing photoreceptor outer segment turnover is the primary mechanism leading to most adult forms of VLs, but in certain clinical settings, including CSC, vitreomacular traction, and PXE, loss of apposition between the photoreceptor tips and the apical surface of the RPE may be the primary mechanism of AVL formation.

In 12 eyes, we observed spontaneous resolution of the AVL. We hypothesize that spontaneous resolution may occur when there has been sufficient photoreceptor loss to allow for the normal mechanisms of photoreceptor outer segment turnover to "catch up," whereby RPE phagocytosis of the abnormal subretinal material may occur. This theory is supported by our observation that spontaneous resolution was seen only in eyes with chronic lesions having areas of ONL thinning overlying the vitelliform material (Figure 5). Visual acuity after resolution of the AVL appeared to correlate with the degree of integrity of the IS/OS junction and ELM at the foveal center.

Many eyes exhibited hypoautofluorescence on FAF in the areas where SD-OCT showed no RPE

and overlying loss of IS/OS junction and ONL thinning. With FA, AVLs typically showed varying degrees of early hypofluorescence in the arteriovenous phase related to blockage of normal choroidal fluorescence by the material in the subretinal space. Hyperfluorescent staining, often mimicking poorly defined occult/Type 1 neovascularization, was typically seen in the late venous and recirculation phases on FA. In this setting, indocyanine green angiography may be useful in select cases to help exclude CNV. Spectral-domain optical coherence tomography is helpful in this context because most of these eyes in our series had no material between the RPE and the Bruch membrane, a finding inconsistent with the presence of Type 1 (sub-RPE) neovascularization. In cases of AVL masquerading as CNV, proper detection is essential to avoid unnecessary and potentially harmful treatment, such as photodynamic therapy or anti–vascular endothelial growth factor injection.[39]

In summary, AVLs may occur in a variety of different clinical entities that share common FA, SD-OCT, nIR reflectance, and FAF features regardless of the underlying clinical diagnosis. We believe that both RPE dysfunction and a lack of apposition between the photoreceptor outer segments and the apical surface of the RPE interfere with the normal phagocytosis and turnover of the photoreceptor outer segments resulting in the accumulation of hyperautofluorescent material within the subretinal space. Additional material, likely representing hyperplastic RPE cells and macrophages containing lipofuscin and melanolipofuscin granules, accumulates in the subretinal space as focal RPE band thickening or bumps on SD-OCT, consistent with observations made in clinicopathologic studies of AVL. In some eyes, this material appears to migrate into the overlying neurosensory retina, a finding also noted in histopathologic studies of eyes with AVLs. Over time, a gradual thinning of the ONL detected on SD-OCT (indicating photoreceptor loss) may allow the normal mechanisms of outer segment turnover to "catch up," resulting in spontaneous resolution of the AVL. Visual acuity correlates best with the integrity of the IS/OS junction and ELM band imaged with SD-OCT at the foveal center. The loss of these outer retinal structures on SD-OCT appears to be a late finding in eyes with AVL and was typically associated with diminished FAF.

Analyzing the pertinent clinical and multimodal imaging findings of AVLs helps clarify the mechanisms involved in their formation and helps in our understanding their natural course. In addition, clinical distinction from masquerading CNV can avert unnecessary interventions and the risks associated with such measures.

Key words: acquired vitelliform lesion, vitelliform detachment, pseudovitelliform, age-related macular degeneration, cuticular drusen, pattern dystrophy, pseudoxanthoma elasticum.

References

1. Allikmets R, Singh N, Sun H, et al. A photoreceptor cell-specific ATP-binding transporter gene (ABCR) is mutated in recessive Stargardt macular dystrophy. Nat Genet 1997;15:236–246.
2. Marmorstein AD, Marmorstein LY, Rayborn M, Wang X, Hollyfield JG, Petrukhin K. Bestrophin, the product of the Best vitelliform macular dystrophy gene (VMD2), localizes to the basolateral plasma membrane of the retinal pigment epithelium. Proc Natl Acad Sci U S A 2000;97:12758–12763.
3. Sun H, Tsunenari T, Yau KW, Nathans J. The vitelliform macular dystrophy protein defines a new family of chloride channels. Proc Natl Acad Sci U S A 2002;99:4008–4013.
4. Gass JD, Jallow S, Davis B. Adult vitelliform macular detachment occurring in patients with basal laminar drusen. Am J Ophthalmol 1985;99:445–459.
5. Gass JDM. A clinicopathological study of a peculiar foveomacular dystrophy. Trans Am Ophthalmol Soc 1974;72:139–156.
6. Gass JDM. Dominantly inherited adult form of vitelliform foveomacular dystrophy. In: fine SL, Owens SL, eds. Management of Retinal Vascular and Macular Disorders. Baltimore, MD: Williams & Wilkins; 1983:182–186.
7. Patrinely JR, Lewis RA, Forn RI. Foveomacular vitelliform dystrophy, adult type: a clinicopathological study including electron microscopic observations. Ophthalmology 1985;92:1712–1718.
8. Fishman GA, Trimble S, Raab MF, Fishman M. Pseudovitelliform macular degeneration. Arch Ophthalmol 1977;95:73–76.
9. Hodes BL, Feiner LA, Sherman SH, Cunningham D. Progression of pseudovitelliform macular dystrophy. Arch Ophthalmol 1984;102:381–383.
10. Vine AK, Schatz H. Adult-onset foveomacular pigment epithelial dystrophy. Am J Ophthalmol 1980;89:680–691.
11. Jaffe GJ, Schatz H. Histopathologic features of adult-onset foveomacular pigment epithelial dystrophy. Arch Ophthalmol 1988;106:958–960.
12. Wells J, Wroblewski J, Keen J, et al. Mutations in the human retinal degeneration slow (RDS) gene can cause either retinitis pigmentosa or macular dystrophy. Nat Genet 1993;3:213–218.
13. Allikmets R, Seddon J, Bernstein PS, et al. Evaluation of the Best disease gene in patients with age-related macular degeneration and other maculopathies. Hum Genet 1999;104:449–453.
14. Dupas B, Tadayoni R, Erginay A, Massin P, Gaudric A. Subfoveal deposits secondary to idiopathic epiretinal membranes. Ophthalmology 2009;116:1794–1798.
15. The Age-Related Eye Disease Study (AREDS): design implications. AREDS report no. 1. Age-Related Eye Disease Study Research Group. Contemp Clin Trials 1999;20:573–600.
16. Zweifel SA, Spaide RF, Curcio CA, Malek G, Imamura Y. Reticular pseudodrusen are subretinal drusenoid deposits. Ophthalmology 2010;117:303.e1–312.e1. Epub ahead of print.
17. Kandula S, Zweifel S, Freund KB. Adult-onset vitelliform detachment unresponsive to monthly intravitreal ranibizumab. Ophthalmic Surg Lasers Imaging In Press.
18. Ghazi NG. Adult-onset foveomacular vitelliform dystrophy: a study by optical coherence tomography. Am J Ophthalmol 2003;135:362–367.

19. Pierro L, Tremolada G, Introini U, Calori G, Brancato R. Optical coherence tomography findings in adult-onset foveomacular vitelliform dystrophy. Am J Ophthalmol 2002;134:675–680.

20. Benhamou N, Souid EH, Zolf R, Coscas F, Coscas G, Soubrane G. Adult-onset foveomacular vitelliform dystrophy: a study by optical coherence tomography. Am J Ophthalmol 2003;135: 362–367.

21. Benhamou N, Messas-Kaplan A, Cohen Y, et al. Adult-onset foveomacular vitelliform dystrophy with OCT 3. Am J Ophthalmol 2004;138:294–296.

22. Querques G, Regenbogen M, Quijano C, Delphin N, Soubrane G, Souied EH. High-definition optical coherence tomography features in vitelliform macular dystrophy. Am J Ophthalmol 2008;146:501–507.

23. Querques G, Regenbogen M, Soubrane G, Souied EH. High-resolution spectral domain optical coherence tomography findings in multifocal vitelliform macular dystrophy. Surv Ophthalmol 2009;54:311–316.

24. Dubovy SR, Hairston RJ, Schatz H, et al. Adult-onset foveomacular pigment epithelial dystrophy. Retina 2000;20: 638–649.

25. Arnold JJ, Sarks JP, Killingsworth MC, Kettle EK, Sarks SH. Adult vitelliform macular degeneration: a clinicopathological study. Eye 2003;17:717–726.

26. Eagle RC, Lucier AC, Bernardino VB, Yanoff M. Retinal pigment epithelial abnormalities in fundus flavimaculatus. Ophthalmology 1980;87:1189–1200.

27. Jaffe GJ, Schatz H. Histopathologic features of adult-onset foveomacular pigment epithelial dystrophy. Arch Ophthalmol 1988;108:958–960.

28. Spaide RF, Noble K, Morgan A, Freund KB. Vitelliform macular dystrophy. Ophthalmology 2006;113:1392–1400.

29. Spaide RF, Koizumi H, Freund KB. Photoreceptor outer segment abnormalities as a cause of blind spot enlargement in acute zonal occult outer retinopathy—complex diseases. Am J Ophthalmol 2008;146:111–120.

30. Smith RT, Chan JK, Busuoic M, Sivagnanavel V, Bird AC, Chong NV. Autofluorescence characteristics of early, atrophic, and high-risk fellow eyes in age-related macular degeneration. Invest Ophthalmol Vis Sci 2006;47:5495–5504.

31. Cruz-Villegas V, Villate N, Knighton RW, Rubsamen P, Davis JL. Optical coherence tomographic findings in acute exudative polymorphous vitelliform maculopathy. Am J Ophthalmol 2003;136;760–763.

32. Parodi MB, Iacono P, Pedio M, et al. Autofluorescence in adult-onset foveomacular vitelliform dystrophy. Retina 2008;28: 801–807.

33. Furino C, Boscia F, Cardascia N, Sborgia L, Sborgia C. Fundus autofluorescence, optical coherence tomography and visual acuity in adult-onset foveomacular dystrophy. Ophthalmologica 2008;222:240–244. Epub ahead of print.

34. Liu J, Itagaki Y, Ben-Shabat S, Nakanishi K, Sparrow JR. The biosynthesis of A2E, a fluorophore of aging retina, involves the formation of the precursor, A2-PE, in the photoreceptor outer segment membrane. J Biol Chem 2000;275:29354–29360.

35. Fishkin N, Jang YP, Itagaki Y, Sparrow JR, Nakanishi K. A2-rhodopsin: a new fluorophore isolated from photoreceptor outer segments. Org Biomol Chem 2003;1:1101–1105.

36. Spaide RF. Autofluorescence from the outer retina and subretinal space. Retina 2008;28:5–35.

37. Laud K, Visaetsilpanonta S, Yannuzzi LA, Spaide RF. Autofluorescence imaging of optic pit maculopathy. Retina 2007;27:116–119.

38. Frangieh GT, Green WR, Fine SL. A histopathologic study of Best's macular dystrophy. Arch Ophthalmol 1982;100:1115–1121.

39. Ergun E, Costa D, Salkter J, Yannuzzi LA, Stur M. Photodynamic therapy and vitelliform lesions. Retina 2004; 24:399–406.